

This is the accepted manuscript made available via CHORUS. The article has been published as:

Statistical correlations of nuclear quadrupole deformations and charge radii

Paul-Gerhard Reinhard and Witold Nazarewicz

Phys. Rev. C **106**, 014303 — Published 7 July 2022

DOI: [10.1103/PhysRevC.106.014303](https://doi.org/10.1103/PhysRevC.106.014303)

Statistical correlations of nuclear quadrupole deformations and charge radii

Paul-Gerhard Reinhard¹ and Witold Nazarewicz²

¹*Institut für Theoretische Physik, Universität Erlangen, Erlangen, Germany*

²*Facility for Rare Isotope Beams and Department of Physics and Astronomy,
Michigan State University, East Lansing, Michigan 48824, USA*

(Dated: June 28, 2022)

Background: Shape deformations and charge radii, basic properties of atomic nuclei, are influenced by both the global features of the nuclear force and the nucleonic shell structure. As functions of proton and neutron number, both quantities show regular patterns and, for nuclei away from magic numbers, they change very smoothly from nucleus to nucleus.

Purpose: In this paper, we explain how the local shell effects are impacting the statistical correlations between quadrupole deformations and charge radii in well-deformed even-even Er, Yb, and Hf isotopes. This implies, in turn, that sudden changes in correlations can be useful indicators of underlying shell effects.

Methods: Our theoretical analysis is performed in the framework of self-consistent mean-field theory using quantified energy density functionals and density-dependent pairing forces. The statistical analysis is carried out by means of the linear least-square regression.

Results: The local variations of nuclear quadrupole deformations and charge radii, explained in terms of occupations individual deformed Hartree-Fock orbits, make an imprint on statistical correlations of computed observables. While the calculated deformations or charge radii are, in some cases, correlated with those of their even-even neighbors, the correlations seem to deteriorate rapidly with particle number.

Conclusions: The statistical correlations between nuclear deformations and charge radii of different nuclei are affected by the underlying shell structure. Even for well deformed and superfluid nuclei for which these observables change smoothly, the correlation range is rather short. This result suggests that the frequently made assumption of reduced statistical errors for the differences between smoothly-varying observables cannot be generally justified.

I. INTRODUCTION

The global behavior of nuclear radii and quadrupole deformations is impacted by the macroscopic properties of nuclear liquid drop such as incompressibility or surface tension. The local behavior, on the other hand, is determined by the microscopic quantal effects such as the nucleonic shell structure, nucleonic pairing, and zero-point correlations due to the particle-vibrational coupling.

The origin of nuclear deformations can be traced back to the nuclear Jahn-Teller effect [1–3], i.e., the spontaneous symmetry breaking of the internal density (or mean-field) due to the coupling of degenerate nucleonic states with collective surface vibrations of the nucleus. The systematic behavior of nuclear quadrupole deformations can be explained through the geometrical properties, or shell topology, of valence proton and neutron orbitals [1, 4]. According to the Hartree-Fock (HF) analysis [5, 6], the main contribution to the quadrupole deformation energy comes from the effective neutron-proton quadrupole interaction that maximizes around the middle of proton and neutron shells. This results in simple patterns [7, 8] of quadrupole deformations which can be well systematized in terms of the promiscuity factor [9] that depends on the distance of Z and N to the closest magic proton and neutron number. Atop this general behavior, local fluctuations in quadrupole deformations may occur due to occupations of individual deformed Nilsson single-particle (s.p.) orbits close to the Fermi level. Depending on their s.p. quadrupole moments, these orbits can increase or decrease total quadrupole

deformations by polarizing the system.

Similar considerations pertain to nuclear charge radii, which are the monopole moments of the nuclear charge density that is dominated by the proton density. Here, the occupations of states with large oscillator quantum numbers dominate the general pattern. The charge radii are also impacted by nuclear deformations in the second order.

The purpose of this Paper is to analyse the local trends of quadrupole deformations and charge radii in terms of statistical correlations between predicted observables in neighboring nuclei. The motivation behind the use of statistical correlation approach can be explained as follows. If the occupations of s.p. levels change smoothly with particle number, and the character of s.p. levels around the Fermi level is similar, one would expect to see large statistical correlations between deformations and radii in close-lying isotopes and isotones. On the other hand, if the intrinsic structure changes rapidly due to, e.g., crossings of s.p. levels with very different quantum numbers, the statistical correlations are expected to be reduced. The isotopic and isotonic trend of statistical correlations can thus be a useful guide in several respects. It indicates changes in shell structure important for model understanding and development. And the information about the typical range of statistical correlation between nuclear observables is important for modeling emulators based on machine learning [10, 11] and assessing statistical errors on differences of observables, e.g., energy differences or differential radii.

This Paper is organized as follows. Section II describes

theoretical models used and the statistical correlation analysis. The results obtained in this study are presented in Sec. III. Finally, the conclusions are presented in Sec. IV.

II. THEORETICAL MODELS

Our analysis has been carried out within the self-consistent nuclear energy density functional method [12]. In our applications, we employ the energy density functionals (EDFs) SV-min [13] and Fy(Δr ,BCS) [14]. Both have been optimized to large experimental calibration datasets of nuclear ground state data by means of the standard linear regression technique, which provides information on uncertainties and statistical correlations between observables.

In SV-min calculations, we employed the standard [14] density-dependent pairing force of mixed type [15]. The generalized pairing functional in the Fy(Δr ,BCS) model additionally depends on the gradient of nucleonic density [16]. In both variants, pairing is treated in the BCS approximation. We do that because the nuclei of interest are well bound; hence, the HF+BCS approach is expected to offer a reasonable description of pairing and high accuracy when computing statistical covariances. Thus we employ Fy(Δr ,BCS) as a BCS-analogue of the original Fy(Δr ,HFB) tuned to exactly the same calibration dataset, particularly the differential charge radii.

Our statistical correlation analysis is based on linear least square regression [13, 17] using the covariance matrices obtained in the course of EDF calibration. The correlation between quantities x and y can be quantified in terms of the bivariate correlation coefficient

$$R_{x,y} = \frac{\text{cov}(x,y)}{\sigma_x \sigma_y}, \quad (1)$$

where σ_x and σ_y are variances of x and y , respectively. The square R^2 is the coefficient of determination (CoD) [18]. It contains information on how well one quantity is determined by another one, within a given model. For our earlier applications of CoD to nuclear observables, see Refs. [19–23]. Values of CoD range from 0 to 1, where 0 implies that, for a given model, the quantities x and y are uncorrelated, whilst 1 denotes that one quantity determines the other completely.

The correlation coefficient (1) is useful when estimating the variance of a difference $x - y$:

$$\sigma_{x-y}^2 = \sigma_x^2 + \sigma_y^2 - 2R_{x,y}\sigma_x\sigma_y. \quad (2)$$

In particular, if the observables x and y are very well correlated ($R_{x,y} \approx 1$), the variance of a difference becomes $\sigma_{x-y} \approx |\sigma_x - \sigma_y|$, i.e., it can be very small if $\sigma_x \approx \sigma_y$.

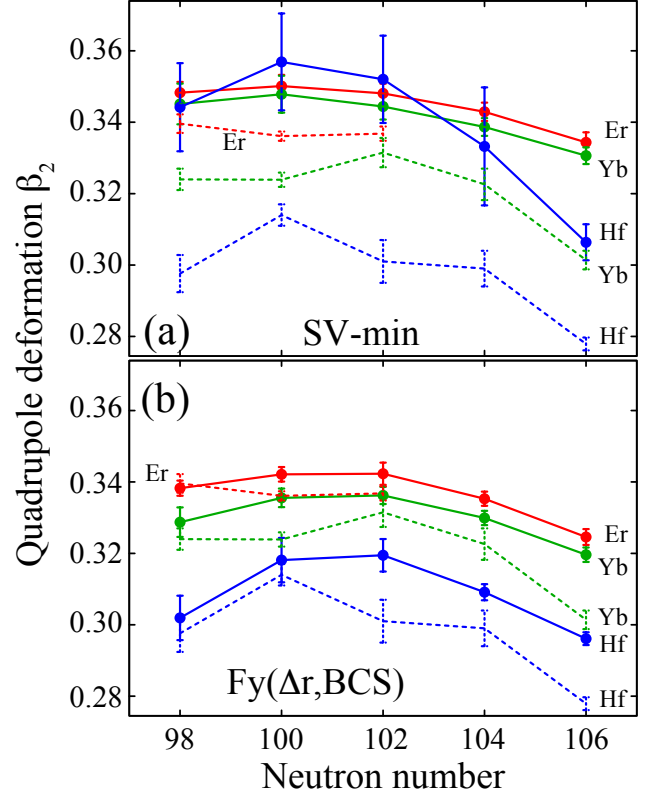


FIG. 1. Proton quadrupole ground-state deformations β_2 for even-even Er, Yb, and Hf isotopes with $98 \leq N \leq 106$ calculated with (a) SV-min and (b) Fy(Δr ,BCS) EDFs compared to empirical values [24] (dashed lines). Statistical model uncertainties and experimental errors are marked.

III. RESULTS

The scope of this Paper is to study the structure of statistical correlations between ground-state deformations and between charge radii in the even-even Er, Yb, and Hf isotopes with $98 \leq N \leq 106$. These nuclei lie in the center of the deformed rare-earth region [24].

The dimensionless quadrupole deformations can be deduced from the calculated proton quadrupole moments

$$\beta_2 = 4\pi \frac{\langle r^2 Y_{20} \rangle}{3ZR^2}, \quad R = 1.2A^{1/3} \text{ fm}. \quad (3)$$

This quantity is directly related to the geometrical shape and thus simplifies comparisons across different nuclei. The average value of the spherical radius R was taken the same as in Ref. [24]. Figure 1 shows the calculated values of β_2 for SV-min and Fy(Δr ,BCS) and compares them to empirical quadrupole deformations extracted from the experimental transition probabilities for the lowest 2^+ states [24]. All isotopes shown in Fig. 1 are very well deformed. Considering the scale of Fig. 1, the agreement between experiment and theory is very reasonable, especially for Fy(Δr ,BCS). This is not so surprising because, as discussed in the introduction, nuclear deformation

properties are dominated by shell topology: all reasonable nuclear models, including macroscopic-microscopic approaches as well as various flavors of nuclear density functional method, are bound to reproduce the deformations of well deformed nuclei. On the other hand, appreciable model differences are expected for transitional isotopes for which the concept of a rigid nuclear deformation is questionable. At the second glance, we see quantita-

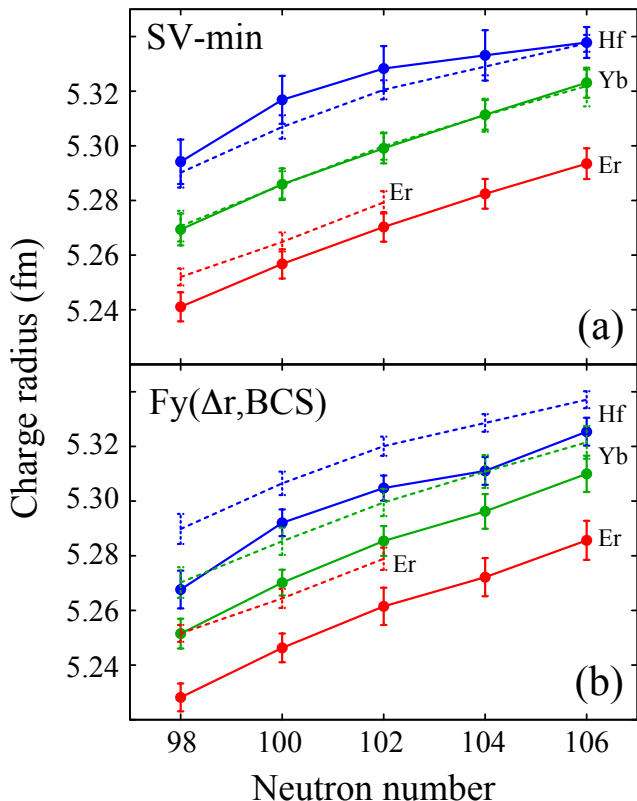


FIG. 2. Charge radii for even-even Er, Yb, and Hf isotopes with $98 \leq N \leq 106$ calculated with (a) SV-min and (b) Fy(Δr ,BCS) EDFs compared to empirical values [25] (dashed lines). Statistical model uncertainties and experimental errors are marked.

tive differences between the two models. The values of β_2 predicted by SV-min are 5%-10% larger and the trend for the Hf isotopes differs visibly. Although the deformation is dominated by shell structure, the final details emerge from an interplay of Coulomb pressure, surface energy, shell effects, and pairing, which all depend on the actual model. We also note that both models tend to predict deformations that are slightly larger than the empirical values. But this minor mismatch is unimportant for our present study which aims at exploring the isotopic and isotonic trends of β_2 and the statistical correlations of β_2 between the isotopes. Coulomb pressure and surface energy change only smoothly with Z and N and this should lead to strong inter-correlations. However, shell structure and pairing can fluctuate, as can already be seen from local variations of β_2 in Fig. 1.

The charge radii R_{ch} of the discussed Er, Yb, and Hf isotopes are displayed in Fig. 2. The radii gradually increase with Z and N , as expected. The fluctuations atop this smooth behavior are seen in the differential radii and their ratios [26]. The charge radii obtained in SV-min are systematically larger than those of Fy(Δr ,BCS). This, together with the results for the quadrupole moments shown in Fig. 1 suggests that the proton densities predicted by SV-min are slightly more radially extended. As in the case of quadrupole deformations, local variations of R_{ch} with N and Z are present.

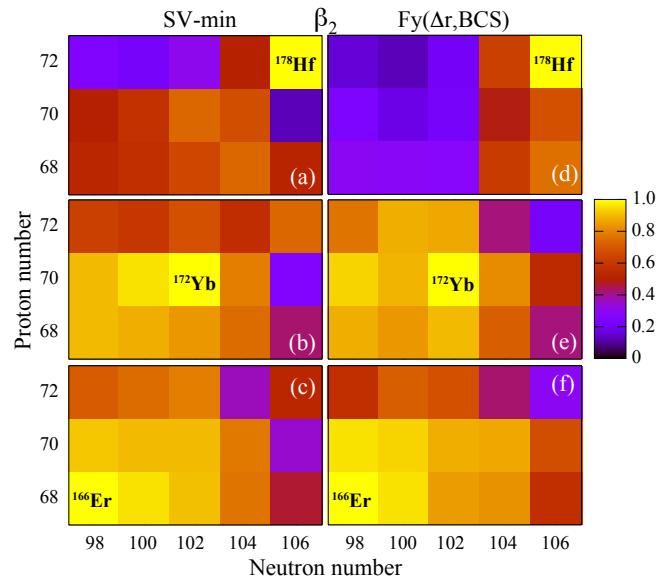


FIG. 3. The CoD $R^2_{\beta_2(Z,N),\beta_2(Z',N')}$ between the quadrupole deformation of the nucleus indicated and β_2 of other Er, Yb, and Hf isotopes with $98 \leq N \leq 106$ calculated with (left) SV-min and (right) Fy(Δr ,BCS) EDFs.

Figure 3 shows a plot of statistical correlations in terms of CoDs between the deformation β_2 in ^{178}Hf (upper panels), ^{172}Yb (middle panels), and ^{166}Er (lower panels) and β_2 values of all other isotopes considered. Interestingly, the quadrupole deformations of ^{172}Yb ($N = 102$) and ^{166}Er ($N = 98$) are well correlated with those of neighboring nuclei, in accordance with expectations. It is only when the neutron number approaches $N = 106$ that the correlation deteriorates. The situation is different for ^{178}Hf — the heaviest nucleus considered. Here, the CoD values are small, even with the nearest neighbors. The inter-nuclei correlations of charge radii are shown in Fig. 4. It is seen that the values of R_{ch} are inter-correlated better than quadrupole deformations. But, similar as in the β_2 case, there are regions of surprisingly low CoDs. Particularly low correlations are predicted for ^{176}Hf in SV-min and ^{170}Hf in Fy(Δr ,BCS) for both β_2 and R_{ch} .

While the general trend is similar for both models, the quantities predicted by SV-min are systematically better correlated than those obtained with Fy(Δr ,BCS). The significant variations of CoDs seen in Figs. 3 and 4 are

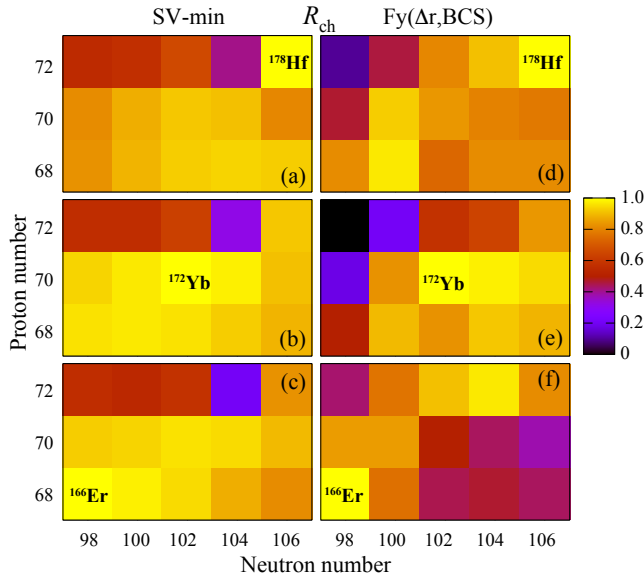


FIG. 4. Similar as in Fig. 3 but for the charge radii.

indicative of shell effects. To confirm that, we must look at the deformed shell structure in this region of nuclei.

Figure 5 shows the single particle (s.p.) energies of ^{172}Yb as functions of β_2 (Nilsson diagram), generated by quadrupole-constrained HF calculations. The s.p. levels are labeled by means of the asymptotic Nilsson quantum numbers $[N_{\text{osc}}n_z\Lambda]\Omega^\pi$ of the stretched harmonic oscillator. The s.p. diagram of Fig. 5 is fairly robust, i.e., it is valid for the deformed Yb region and it weakly depends on the model used (cf. Ref. [27] for the modified harmonic oscillator and Woods-Saxon s.p. diagrams in this region or Ref. [28] for Gogny-model calculations).

The proton shell structure in the deformed Yb region is defined by the pronounced deformed subshell closure at $Z = 70$. At lower deformations, this gap is closed by the upsloping (oblate-driving) extruder orbitals $[404]7/2^+$ and $[402]5/2^+$. At larger deformations, $\beta_2 > 0.33$, the downsloping (prolate-driving) $[541]1/2^-$ intruder level becomes occupied at $Z = 72$. Below the $Z = 70$ gap, there appear two close-lying Nilsson levels: oblate-driving $[411]1/2^+$ and prolate-driving $[532]7/2^-$, which close another deformed gap at $Z = 66$. These levels cross at $\beta_2 \approx 0.30$ for $\text{Fy}(\Delta r, \text{BCS})$ and $\beta_2 \approx 0.39$ for SV-min.

The neutron shell structure is characterized by the deformed gap at $N = 104$. This gap is closed from the above by the oblate-driving $[514]7/2^-$ and the unique-parity $[624]9/2^+$ levels, which cross at $\beta_2 \approx 0.35$. From the below, the $N = 104$ gap is bounded by the prolate-driving unique-parity $[633]7/2^+$ level and the oblate-driving $[512]5/2^-$ level, which cross at $\beta_2 \approx 0.32$ for SV-min and $\beta_2 \approx 0.28$ for $\text{Fy}(\Delta r, \text{BCS})$.

The deformed shell structure is defined by the occupations of s.p. orbits shown in Fig. 5. In the presence of nucleonic pairing, the s.p. occupations change grad-

ually with particle number leading to smooth variations of nuclear observables. If pairing is weak, the transitions between intrinsic HF configurations are sharp and the underlying picture becomes diabatic. Consequently, large pairing is expected to increase correlations between observables belonging to different nuclei. Figure 6 displays proton and neutron pairing energies of the nuclei considered. The large deformed gap at $Z = 70$ gives rise to very weak proton pairing in the Yb isotopes. The variations of neutron pairing are appreciable; they reach a minimum at the deformed neutron closure $N = 104$.

The systematic trend of β_2 in Fig. 1 can be traced back to the s.p. diagram of Fig. 5. The quadrupole deformations of Er and Yb isotopes are close as the quadrupole polarization effects of $[411]1/2^+$ and $[523]7/2^-$ proton levels compensate. The reduction of β_2 in the Hf isotopes in $\text{Fy}(\Delta r, \text{BCS})$ and for $N > 100$ in $\text{Fy}(\Delta r, \text{BCS})$ can be attributed to the occupations of the oblate-driving $[404]7/2^+$ and $[402]5/2^+$ proton levels. The large value of β_2 in ^{172}Hf predicted in SV-min is due to the filling of the $\pi[541]1/2^-$ level. Finally, a reduction of β_2 when approaching $N = 106$ reflects the filling of oblate-driving $[512]5/2^-$ and $[514]7/2^-$ neutron levels. When it comes to the charge radii, the local increase of R_{ch} around $N = 100, 102$ can be associated with the occupation of the neutron intruder level $[633]7/2^+$.

Having established the consistency of trends in β_2 and R_{ch} with the deformed shell-structure, let us see whether the details of the Nilsson plot will be reflected in the correlation systematics of Figs. 3 and 4. Microscopically, the energies and wave functions extruder and intruder Nilsson states (including the unique-parity states) impacting the configuration changes of the deformed Er, Yb, and Hf isotopes are strongly influenced by the surface and spin-orbit terms of the EDFs [16, 29]. Consequently, these parts of the EDFs are expected to impact statistical correlations between computed surface deformations and charge radii.

Let us begin discussion from the CoD pattern of β_2 . As seen in Figs. 3(a) and 3(d), β_2 in ^{178}Hf is poorly correlated with quadrupole deformations of other nuclei. This nucleus is predicted to have a reduced value of $\beta_2 \approx 0.3$ compared to other systems. At this deformation, the occupation of the $[404]7/2^+$ and $[402]5/2^+$ extruder orbits is 1.2-1.3, while these orbits are practically empty in the Yb and Er isotopes, as well as in $^{170,172,174}\text{Hf}$ in SV-min in which the intruder level $[541]1/2^-$ becomes occupied at $\beta_2 > 0.34$. Moreover, the neutron structure of ^{178}Hf involves the occupation of the $[514]7/2^-$ and $[624]9/2^+$ orbitals, which are empty in lighter isotopes with $N < 104$. All these configuration changes involve deformation-driving orbitals and result in reduced CoD values.

Moving on to Figs. 3(b) and 3(e), the quadrupole deformation of ^{172}Yb is correlated fairly well with the β_2 values of lighter systems. This nucleus is calculated to have $\beta_2 \approx 0.34$. The decrease of correlations at $N = 106$ can be associated with the filling of the neutron $[624]9/2^+$

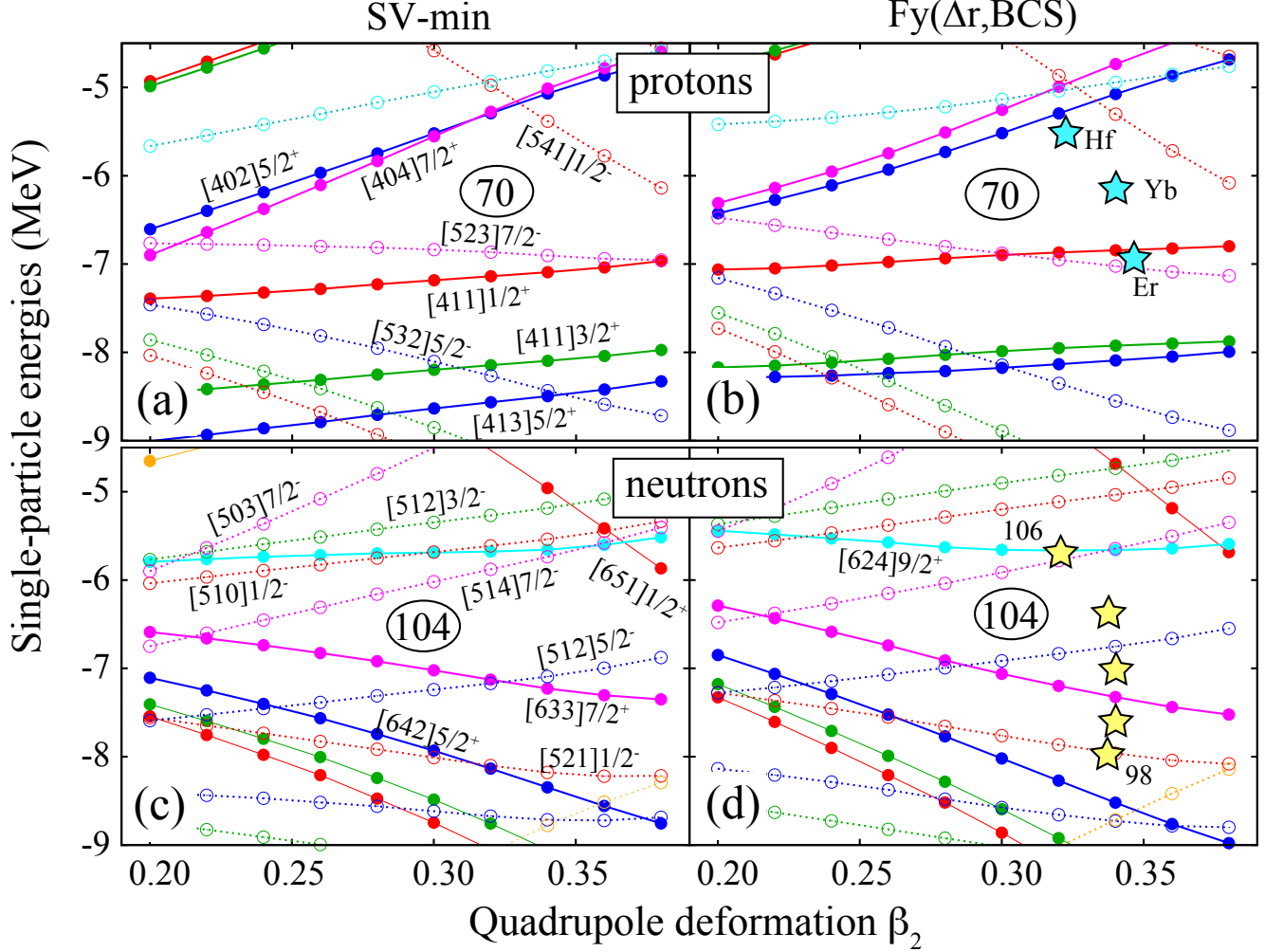


FIG. 5. Proton (top) and neutron (bottom) single-particle energies of ^{172}Yb calculated with SV-min (left) and Fy(Δr ,BCS) (right) EDFs as functions of the proton quadrupole deformation. The asymptotic Nilsson labels $[N_{osc}n_z\Lambda]\Omega^\pi$ are marked. The positions of proton Fermi levels for the $N = 102$ isotones is indicated by stars in panel (b) and the neutron Fermi levels along the Yb isotopic chain - in panel (d).

intruder level. The situation shown in Figs. 3(c) and 3(f) for ^{166}Er is reminiscent of that for ^{172}Yb : the decrease of β_2 -correlations is seen for $N = 106$ (neutron $[624]9/2^+/[514]7/2^-$ occupation) and $Z = 72$ (proton $[541]1/2^-$ or $[404]7/2^+/[402]5/2^+$ occupation).

The pattern of inter-nuclear R_{ch} -correlations shown in Fig. 4 differs from that of β_2 correlations as the charge radii are expected to primarily depend on the radial properties of occupied states, hence N_{osc} . Those are $N_{osc} = 5$ proton levels $[523]7/2^-$ and $[541]1/2^-$ and $N_{osc} = 6$ neutron levels $[642]5/2^+$, $[633]7/2^+$, and $[624]9/2^+$.

IV. CONCLUSIONS

In this Paper, we investigated inter-correlations between observables in neighboring nuclei which exhibit smooth trends as a function of proton or neutron num-

ber. To this end, we selected 15 well deformed even-even Er, Yb, and Hf isotopes in the middle of the well deformed rare earth region. The spherical shell structure in these nuclei is much fragmented by deformation effects, and the single-particle occupations are smoothed out by nucleonic pairing. The calculated quadrupole moments and charge radii vary gradually with Z and N , which would intuitively suggest strong inter-correlations. To check this hypothesis, we carried out statistical correlation analysis based on covariance matrices obtained in the least-square optimization. As measure for correlations, we use the coefficient of determination which is the square of the normalized covariance between two observables.

The calculated CoD diagrams show patterns that are surprisingly localized as compared to the smooth trends of observables. These local variations of CoDs reflect the underlying deformed shell structure and changes of

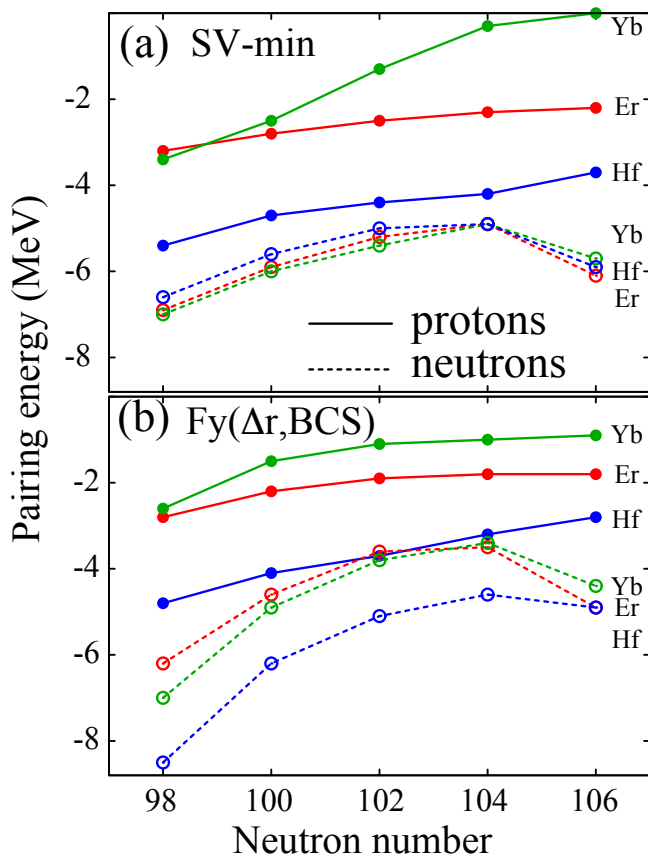


FIG. 6. Proton (solid lines) and neutron (dashed lines) pairing energies (expectation values of the pairing EDF) for even-even Er, Yb, and Hf isotopes with $98 \leq N \leq 106$ calculated with (a) SV-min and (b) Fy(Δr ,BCS) EDFs.

single-particle configurations due to crossings of s.p. levels, especially high- N_{osc} intruder and oblate-driving intruder levels. In fact, the correlation range is fairly short. In some extreme cases, e.g., quadrupole deformation of ^{178}Hf in Fy(Δr ,BCS), the observables are hardly correlated with the values in neighboring nuclei. This finding is consistent with the results for separation energies using Bayesian machine learning [10, 11]. Our results suggest that the frequently made assumption of strong correlations between smoothly-varying observables, which must result in reduced statistical errors of their differences, cannot always be justified. The recommended way to compute statistical uncertainties on theoretical predictions and their differences, however smooth they are, remains the standard way, namely by means of covariances (or posterior distribution functions) obtained in the course of least-squares or Bayesian calibration, see, e.g., Refs. [13, 30].

Acknowledgements.—This material is based upon work supported by the U.S. Department of Energy, Office of Science, Office of Nuclear Physics under award numbers DE-SC0013365 and by the National Science Foundation CSSI program under award number 2004601 (BAND collaboration). We also thank the RRZE computing center of the Friedrich-Alexander university Erlangen/Nürnberg for supplying resources for that work.

- [1] P.-G. Reinhard and E. Otten, “Transition to deformed shapes as a nuclear Jahn-Teller effect,” *Nucl. Phys. A* **420**, 173 (1984).
- [2] W. Nazarewicz, “Nuclear deformations as a spontaneous symmetry breaking,” *Int. J. Mod. Phys. E* **02**, 51–69 (1993).
- [3] W. Nazarewicz, “Microscopic origin of nuclear deformations,” *Nucl. Phys. A* **574**, 27–49 (1994).
- [4] G. Bertsch, “Remark on Y4 moments,” *Phys. Lett. B* **26**, 130–131 (1968).
- [5] J. Dobaczewski, W. Nazarewicz, J. Skalski, and T. Werner, “Nuclear deformation: A proton-neutron effect?” *Phys. Rev. Lett.* **60**, 2254–2257 (1988).
- [6] T. Werner, J. Dobaczewski, M. Guidry, W. Nazarewicz, and J. Sheikh, “Microscopic aspects of nuclear deformation,” *Nucl. Phys. A* **578**, 1–30 (1994).
- [7] J. Jänecke, “Simple parameterization of nuclear deformation parameters,” *Phys. Lett. B* **103**, 1–4 (1981).
- [8] W. Nazarewicz and I. Ragnarsson, “Nuclear deformations,” in *Handbook of Nuclear Properties*, edited by D. Poenaru and W. Greiner (Clarendon Press, Oxford, Oxford, 1996) pp. 80–130.
- [9] R. F. Casten, D. S. Brenner, and P. E. Haustein, “Valence p-n interactions and the development of collectivity in heavy nuclei,” *Phys. Rev. Lett.* **58**, 658–661 (1987).
- [10] L. Neufcourt, Y. Cao, W. Nazarewicz, and F. Viens, “Bayesian approach to model-based extrapolation of nuclear observables,” *Phys. Rev. C* **98**, 034318 (2018).
- [11] L. Neufcourt, Y. Cao, S. A. Giuliani, W. Nazarewicz, E. Olsen, and O. B. Tarasov, “Quantified limits of the nuclear landscape,” *Phys. Rev. C* **101**, 044307 (2020).
- [12] M. Bender, P.-H. Heenen, and P.-G. Reinhard, “Self-consistent mean-field models for nuclear structure,” *Rev. Mod. Phys.* **75**, 121–180 (2003).
- [13] P. Klüpfel, P.-G. Reinhard, T. J. Bürvenich, and J. A. Maruhn, “Variations on a theme by Skyrme: A systematic study of adjustments of model parameters,” *Phys. Rev. C* **79**, 034310 (2009).
- [14] P.-G. Reinhard and W. Nazarewicz, “Toward a global description of nuclear charge radii: Exploring the Fayans energy density functional,” *Phys. Rev. C* **95**, 064328 (2017).
- [15] J. Dobaczewski, W. Nazarewicz, and P.-G. Reinhard, “Pairing interaction and self-consistent densities in neutron-rich nuclei,” *Nucl. Phys. A* **693**, 361–373 (2001).
- [16] S. A. Fayans, S. V. Tolokonnikov, E. L. Trykov, and

- D. Zawischa, “Nuclear isotope shifts within the local energy-density functional approach,” *Nucl. Phys. A* **676**, 49 (2000).
- [17] J. Dobaczewski, W. Nazarewicz, and P.-G. Reinhard, “Error estimates of theoretical models: a guide,” *J. Phys. G* **41**, 074001 (2014).
- [18] S. A. Glantz, B. K. Slinker, and T. B. Neilands, *Primer of Applied Regression & Analysis of Variance* (McGraw Hill, 1990).
- [19] J. Erler and P.-G. Reinhard, “Error estimates for the Skyrme-Hartree-Fock model,” *J. Phys. G* **42**, 034026 (2015).
- [20] P.-G. Reinhard, “Estimating the relevance of predictions from the Skyrme-Hartree-Fock model,” *Phys. Scr.* **91**, 023002 (2016).
- [21] B. Schuetrumpf, W. Nazarewicz, and P.-G. Reinhard, “Central depression in nucleonic densities: Trend analysis in the nuclear density functional theory approach,” *Phys. Rev. C* **96**, 024306 (2017).
- [22] P.-G. Reinhard, “Nuclear density-functional theory and fission of super-heavy elements,” *Eur. Phys. J A* **54**, 13 (2018).
- [23] P.-G. Reinhard, W. Nazarewicz, and R. F. Garcia Ruiz, “Beyond the charge radius: The information content of the fourth radial moment,” *Phys. Rev. C* **101**, 021301(R) (2020).
- [24] B. Pritychenko, M. Birch, B. Singh, and M. Horoi, “Tables of E2 transition probabilities from the first 2+ states in even-even nuclei,” *At. Data Nucl. Data Tables* **107**, 1–139 (2016).
- [25] I. Angeli and K. P. Marinova, “Table of experimental nuclear ground state charge radii: An update,” *At. Data Nucl. Data Tables* **99**, 69–95 (2013).
- [26] J. Hur, D. P. L. Aude Craik, I. Counts, E. Knyazev, L. Caldwell, C. Leung, S. Pandey, J. C. Berengut, A. Geddes, W. Nazarewicz, P.-G. Reinhard, A. Kawasaki, H. Jeon, W. Jhe, and V. Vuletić, “Evidence of two-source King plot nonlinearity in spectroscopic search for new boson,” *Phys. Rev. Lett.* **128**, 163201 (2022).
- [27] R. Bengtsson, J. Dudek, W. Nazarewicz, and P. Olanders, “A systematic comparison between the Nilsson and Woods-Saxon deformed shell model potentials,” *Phys. Scr.* **39**, 196–220 (1989).
- [28] http://www-phynu.cea.fr/science_en_ligne/carte_potentiels_microscopiques/carte_potentiel_nucleaire_eng.htm.
- [29] J. Dobaczewski, W. Nazarewicz, and M.V. Stoitsov, “Nuclear ground-state properties from mean-field calculations,” *Eur. Phys. J. A* **15**, 21–26 (2002).
- [30] J. D. McDonnell, N. Schunck, D. Higdon, J. Sarich, S. M. Wild, and W. Nazarewicz, “Uncertainty quantification for nuclear density functional theory and information content of new measurements,” *Phys. Rev. Lett.* **114**, 122501 (2015).